ISSN 0001-4370, Oceanology, 2016, Vol. 56, No. 4, pp. 515–526. © Pleiades Publishing, Inc., 2016.
Original Russian Text © A.B. Demidov, S.A. Mosharov, V.A. Artemyev, A.N. Stupnikova, U.V. Simakova, S.V. Vazyulya, 2016, published in Okeanologiya, 2016, Vol. 56, No. 4, pp. 563–576.

MARINE BIOLOGY

Depth-Integrated and Depth-Resolved Models of Kara Sea Primary Production

A. B. Demidov[a], S. A. Mosharov[a, b], V. A. Artemyev[a], A. N. Stupnikova[a], U. V. Simakova[a], and S. V. Vazyulya[a]

[a] *Shirshov Institute of Oceanology, Russian Academy of Sciences, Moscow, 117218 Russia*
[b] *Bauman Moscow State Technical University, Moscow, 105005 Russia*
e-mail: demspa@rambler.ru

Received February 15, 2014

Abstract—Primary production (PP) models of the Kara Sea are developed based on data collected on fall expeditions (September–October 1993, 2007, and 2011) and their precision assessment utilizes the dataset collected in September 2013. The algorithms for different model types (depth-integrated and depth-resolved) are compared. The depth-resolved model performs slightly better than the depth-integrated one (the root-mean-square-difference (RMSD) are 0.29 and 0.31, respectively). These algorithms utilize the daily assimilation number (DAN) and photosynthetic efficiency (ψ) as the model coefficients, and surface chlorophyll *a* (chl *a*) and photosynthetically active radiation (PAR) as input variables. These algorithms perform better than the models that use chl *a* alone. Our results suggest that an increase in the performance of the Kara Sea PP models depends on the input of the photophysiological characteristics of phytoplankton (DAN and ψ) and PAR. To a lesser extent, this concerns the advantages of the depth-resolved model over the depth-integrated one. The constructed region-specific Kara Sea PP models combined with satellite-derived chl *a* and PAR can be used to estimate annual values and long-term variation of PP in hydrologically and hydrochemically similar waters of the Arctic Ocean.

DOI: 10.1134/S0001437016040020

INTRODUCTION

One of the major problems in studying and assessing oceanic primary production (PP) is that field studies give PP data (see Table 1 for explanation of symbols and abbreviations) for a particular site and a particular time but do not allow for study of the spatiotemporal variation, detection of large-scale and long-term trends, and assessment of annual values to a sufficient accuracy [20]. Solution of these problems using experimental shipboard data requires considerable extrapolation [19, 46], which interferes with sufficiently accurate quantitative determination of PP variation on a large spatiotemporal scale. This problem is solvable with biooptical remotely sensed data, which provides information about various characteristics of the ocean surface (for example, surface chlorophyll and temperature as well as photosynthetically active radiation, PAR) for large water areas with a high time resolution [23, 51, 52, 56]. One of the approaches to using satellite data implies the construction of PP computation algorithms and assessment of their precision based on an experimental dataset with the surface characteristics as model parameters [16, 25, 61].

PP models are classified in different ways. Without any claim of completeness, several types of models are distinguished depending on their main parameters:

(1) models based on the chlorophyll concentration (Chl-based models), which utilize the water column optimum chlorophyll specific carbon fixation rate, P^b_{opt} [for example, 16];

(2) models based on phytoplankton carbon content (C-based models) and utilizing the phytoplankton growth rate [15, 75]; and

(3) models utilizing water circulation and biogeochemistry (GCM-based models) [34, 45, 53, 73]. The classification based on depth and solar radiation wavelength resolutions fall into the WIDI (wavelength- and depth-integrated), WIDR (wavelength-integrated and depth-resolved), and WRDR (wavelength- and depth-resolved) types [25].

The fit of model computations to field data (model precision) for the listed types of algorithms has been assessed on global and regional scales [22, 25, 32, 65, 66]. The resulting conclusions state that (a) the precision of the models is independent of its complexity, i.e., the number of input variables and depth and wavelength resolutions, and (b) the models overestimate or underestimate the annual PP by approxi-

Table 1. Used variables, designations, and abbreviations

Variable	Unit of measurement	Designation
IPP_{meas}	mg C/m^2/day	Measured integrated primary production
IPP_{mod}	mg C/m^2/day	Integrated primary production calculated using model
PP_z	mg C/m^3/day	Measured primary production in layer z
Chl_0	mg/m^3	Surface chlorophyll *a* concentration
Chl_z	mg/m^3	Chlorophyll *a* concentration in layer z
Chl_{ph}	mg/m^2	Chlorophyll *a* concentration in photosynthetic layer
k		Index of chl *a* vertical distribution (Chl_{phs}/Chl_0)
P^b_{opt}	mg C/mg chl *a*/h	Water column maximum chlorophyll specific carbon fixation rate
P^b_z	mg C/mg chl *a*/h	Chlorophyll specific carbon fixation rate at depth z
P^b	mg C/mg chl *a*	Average daily chlorophyll specific carbon fixation rate in water column
ψ	g C/mg chl *a*/Ein	Photosynthetic efficiency in water column
I_0 (PAR)	Ein/m^2/day	Subsurface photosynthetically active radiation
I_z	%	Relative irradiance in layer z
Z_s	m	Secchi disk depth
T_0	°C	Surface temperature
K_d	m^{-1}	Diffusion attenuation coefficient for downwelling irradiance
ζ		Optical depth ($K_d z$)
Symbols and abbreviations		
PP		Primary production
IPP		Depth-integrated primary production (the primary production in water column)
chl *a*		Chlorophyll *a*
PAR		Photosynthetically active radiation
UML		Upper mixed layer
SCM		Subsurface chlorophyll maximum
DOM		Dissolved organic matter
POM		Particulate organic matter

mately two fold. These conclusions are also applicable to models constructed for the Arctic Ocean [40] and algorithms adapted for this region used for assessing the annual PP as well as its seasonal and interannual dynamics [39, 63].

It is known that the algorithms for integrated PP (IPP) assessment based on data for the overall World Ocean decrease in accuracy when applied on a regional scale [18, 22, 66, 68]. Thus, a way to increase the precision of PP models is to design the regional algorithms based on experimental datasets for local areas and seas with specific hydrophysical, hydrooptical, and biogeochemical features. The Kara Sea is such a region, owing to the specifics of synthesis of organic matter. The discharges of the Ob and Yenisei rivers, with an annual average volume of about 1100 km^3 [71], account for approximately 55% of the total river discharge to all Russian Arctic seas and over one-third of the total freshwater discharge to the Arctic Ocean [36]. The large freshwater inflow forms pronounced water column stratification as well as narrow frontal zones between river and sea waters. As a result, the structure–function characteristics of pelagic plankton communities are differentiated by sea area and water column [7, 8, 33, 41, 47, 55]. The steep gradients of the physicochemical properties of a waterbody, first and

foremost, salinity and concentrations of suspended and dissolved matter, make up the specific features of both biotic and abiotic factors that determine the conditions of phytoplankton PP. These specific features include temperature and water transparency, which are low year round, and as a consequence of the former, a thin photosynthetic layer (on the average, 22 m) and a high chlorophyll *a* (chl *a*) concentration (on average, >1 mg/m^3) over the pycnocline [1, 6]. Another specific feature of the Kara Sea is its relatively small depth, which also determines the specific features in the supply of major nutrients to the photosynthetic layer. The average depth of the sea is 110 m; of the shelf area, 56 m [24, 42].

The currently available Kara Sea PP estimates are either based on calculations utilizing chl *a* concentration alone [2, 39] or models adapted for the Arctic but initially constructed for other regions of the World Ocean, in particular, for Antarctica [63]. These estimates can significantly differ from field data [27]. One of the likely reasons for these discrepancies is that the phytoplankton photoadaptive parameters (such as assimilation activity and photosynthetic efficiency) and PAR are omitted in regression models, which relate chl *a* concentration to PP in the water column. As shown recently [27], these parameters to a considerable degree determine the Kara Sea PP values, at least in the fall. Another factor is that specific features in the chl *a* vertical distribution are ignored. Thus, an adequate estimate for the Kara Sea IPP requires regional models that take into account the specific photophysiological features of phytoplankton and its vertical distribution. Comparison of the precision of different model types is of independent methodological importance.

For all these reasons, we have formulated the following goals for our study: (a) to construct regional models of the Kara Sea IPP of WIDI and WIDR types utilizing chl *a* concentration, PAR, assimilation number, and photosynthetic efficiency as input variables; (b) to assess the precisions of these models using independent data, i.e., the measured dataset that was not used for model development; (c) to assess the role of chl *a* vertical distribution in increasing the model accuracy; and (d) to compare the efficiency of different model types.

MATERIALS AND METHODS

Data sources, sampling, and subregions of the Kara Sea. The database analyzed in this study compiles the data of three ecosystem expeditions to the Kara Sea: the 49th voyage of R/V *Dmitrii Mendeleev* (August–September 1993) and 54th and 59th voyages of the R/V *Akademik Mstislav Keldysh* (September 2007 and September–October 2011, respectively). The study areas and locations of stations were described earlier [1, 6], while Fig. 1a shows a consolidated map of sampling sites for these expeditions. In total, the chl *a* concentration was recorded at 113 stations, and PP, at 85. The PP, chl *a*, and PAR data used for assessment of the models' capacity were collected at station 31 during the 125th voyage of the R/V Professor Shtokman in August–September 2013 (Fig. 1b).

The sampling procedure was recently described in detail [27]. The locations of stations were selected based on hydrophysical and hydrooptical surveys with a Rybka multiparametric scanning probe and flow-through fluorometer designed at the Institute of Oceanology, Russian Academy of Sciences. The locations of stations were selected to maximally cover the studied water area with experimental points and to obtain the most comprehensive characteristics of gradient frontal zones. The sampling layers were determined after preliminary probing of temperature, conductivity, and fluorescence with Seabird Electronics CTD probes (SBE-19 and SBE-32).

To assay the chl *a* concentration, water was sampled with the plastic bottles of a Carousel Water Sampler from horizons 6–9 of the upper 100-m layer. The surface water at these stations was sampled with a plastic bucket with simultaneous closing of the plastic bottles near the surface.

The measured chl *a* concentration, PP, PAR, and water density were partitioned according to trophic gradations. The Chl_0 values [54, 74] in the following ranges were selected as the characteristics of water productivity: (I) 0.1–0.5 mg/m^3, (II) 0.5–1.0 mg/m^3, (III) 1.0–2.0 mg/m^3, and (IV) >2 mg/m^3. The procedure used for distinguishing Kara Sea water types is described in detail for considering vertical variations in the PP and chl *a* concentration [4].

Measuring PP, chlorophyll concentration, incident and underwater irradiance. The method and experimental schemes for assessing PP were described earlier in detail [1, 6] and summarized by Demidov et al. [27]. In all expeditions, PP was measured with radiocarbon modification of the light-and-dark-bottle technique [70]. Chl *a* concentration was determined spectrophotometrically [43, 67] or fluorometrically [44]. These data were used in constructing the IPP models.

The PP values used in assessment of the model's efficiency were obtained in experiments in an ICES incubator [26]. Probes labeled with $H^{14}CO_3^-$ were incubated in artificial illumination for 3–4 h. P^b was calculated for 12 light levels. The results were used to construct photosynthetic light curves, which were approximated by an exponential function [58]:

$$P^b = P^b_{max}(1 - \exp(-\alpha I / P^b_{max})) \times \exp(-\beta I / P^b_{max}), \quad (1)$$

where P^b_{max} is the maximal chlorophyll specific carbon fixation rate (mg C/mg chl *a*/h); α is the photosynthetic efficiency index, the initial slope of the light curve (mg C/mg chl *a*/h/Ein/m^2/s); *I*, light intensity

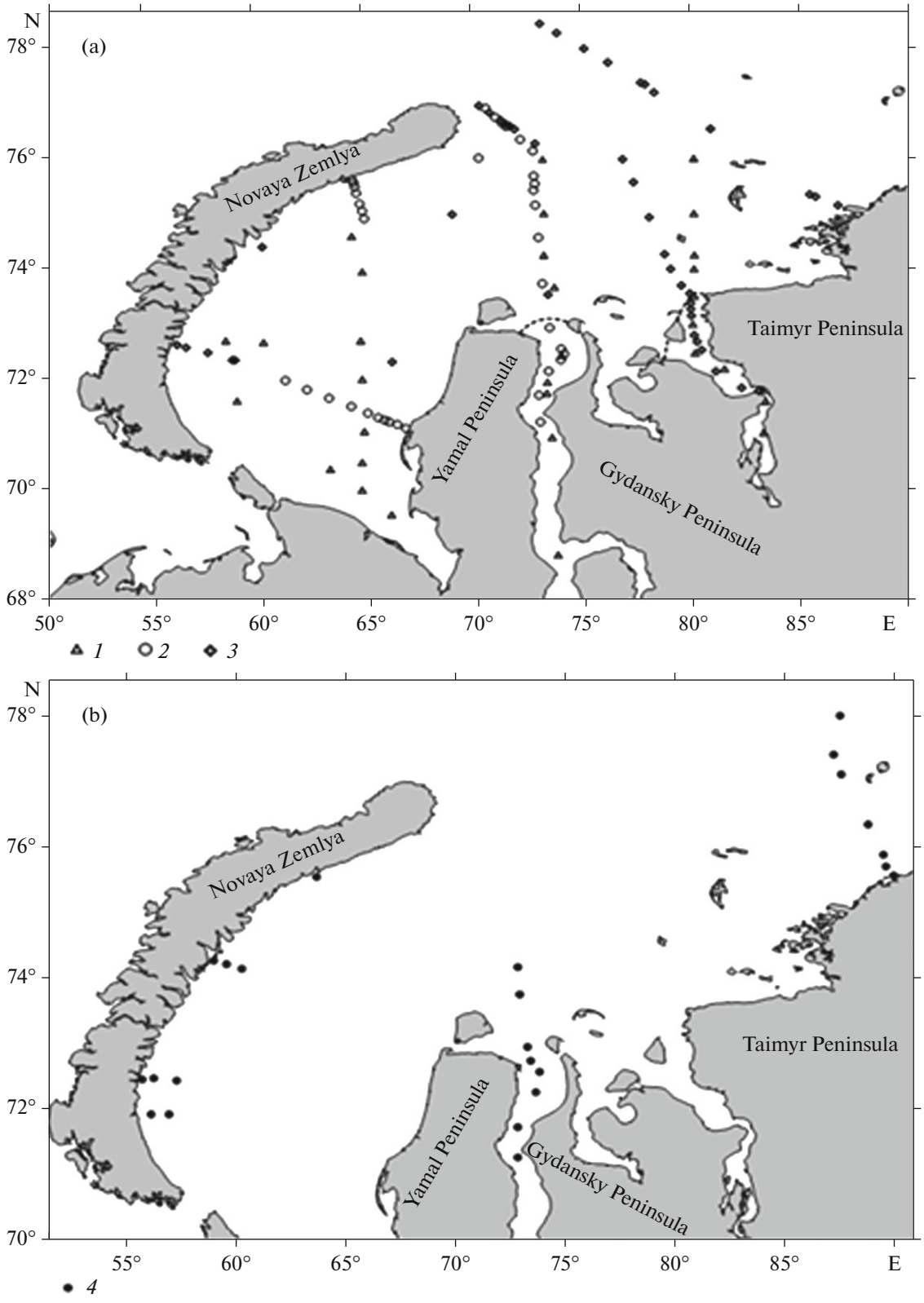

Fig. 1. Location of stations for recoding phytoplankton production parameters for (a) development and (b) assessment of model performance: (1) 49th voyage of R/V *Dmitrii Mendeleev*; (2) 54th voyage of the R/V *Akademik Mstislav Keldysh*; (3) 59th voyage of the R/V *Akademik Mstislav Keldysh*; and (4) 125th voyage of the R/V *Professor Shtokman*.

Table 2. Description of models and data sources

Name	Definition	Model type	Input variables	Sources	Regional specificity
Chl_0_reg	Regression algorithm based on correlation between Chl_0 and IPP	WIDI	Chl_0	This paper	Kara Sea
Ψ-Mod	Model based on PP, chl *a*, and PAR values average for the region	WIDI	Chl_0 and PAR	This paper	Kara Sea
Chl_z_reg	Regression algorithm based on the correlation between Chl_z and PP_z in the Kara Sea	WIDR	Chl_z	This paper	Kara Sea
KSDRM	Kara Sea depth-resolved model	WIDR	Chl_0 and PAR	This paper	Kara Sea

WI, wavelength-integrated; DI, depth-integrated; and DR, depth-resolved.

(Ein/m^2/s); and β, the light attenuation parameter, the negative slope of the light curve (mg C/mg chl *a*/h/Ein/m^2/s).

The incident irradiance was measured with a pyranometer [1] or an LI-190SA (LI-COR) incident radiation sensor in the PAR range. The recorded data were automatically integrated in an LI-1400 unit over 5-min intervals (Ein/m^2) over the day, stored in this unit, and later used to compute the incident radiation for the exposure period of the experimental bottles to assess the PP in the overall light period for a particular date.

The vertical light attenuation coefficient (K_d) was determined with an alphameter. In the absence of underwater hydrooptical measurements, the K_d values were calculated using the empirical dependence of the light attenuation coefficient on the relative transparency according to a Secchi disk (Z_s), recorded in August–September 1993 [1, 27]:

$$K_d = (0.81 \ln Z_s + 0.79)/Z_s. \quad (2)$$

The K_d values at the stations where Z_s was not measured were calculated from Chl_0:

$$K_d = 0.13 \ln Chl_0 + 0.37. \quad (3)$$

In addition, K_d was calculated using Z_s as the conversion factor:

$$K_d = x/Z_s, \quad (4)$$

where x varies from 1.7 to 2.3 (1.7 [64], 2.3 [35], and 1.84 [29]). For our calculations, we took the mean value, so that

$$K_d = 1.95/Z_s. \quad (5)$$

When both Z_s and Chl_0 data were available, all three methods were used to calculate the mean K_d.

IPP model validation. Linear regression equations were used to approximate the correlation between the measured IPP values and the values calculated using the developed models. The degree of correlation between IPP_{mod} and IPP_{meas} was estimated according to determination coefficient (R^2). The resulting regressions were compared to the optimal correspondence line (1 : 1). RMSD was used to assess the model's performance. RMSD characterizes the difference between the IPP_{mod} and IPP_{meas} logarithm values and comprises both bias and random error [28, 72]:

$$\mathrm{RMSD} = \left(\frac{1}{N} \sum_{i=1}^{N} \Delta(i)^2 \right)^{1/2}, \quad (6)$$

where the difference between the measured and calculated values, $\Delta(i)$, is

$$\Delta(i) = \log_{10}(IPP_{meas}(i)) - \log_{10}(IPP_{mod}(i)). \quad (7)$$

The log normalized RMSD was used previously to assess the overall model performance (Primary Production Algorithm Round Robin, PPARR) [22, 32, 65, 66]. Models with a low RMSD value are more effective than algorithms with a high RMSD value. An RMSD value close to 0.3 indicates approximately twofold overestimation or underestimation of the calculated values compared with the measured data. In addition, we calculated the mean biases (B) for each model in order to assess the overestimation or underestimation of IPP_{meas} where

$$B = \overline{\log(IPP_{mod})} - \overline{\log(IPP_{meas})}. \quad (8)$$

RESULTS

We have considered approaches to parameterizing the Chl-based WIDI and WIDR models developed using the Kara Sea dataset. The models are briefly described in Table 2.

Empirical dependence between the surface chlorophyll and water column IPP. The chl *a* concentration is considered in the simplest models as a PP characteristic in the water column [30, 69]. The IPP is frequently calculated according to remote sensing using the chl *a* concentration in the layer, which forms an upward radiation flux, recorded by ocean color scanners; note that the chl *a* concentration is close to Chl_0. This has been confirmed for the Kara Sea when studying the

conditions for PP formation [27]. Surface chlorophyll in earlier works was used to assess the IPP in Russian Arctic seas [2] and in the World Ocean [3].

Using the data for the Kara Sea in the fall, we observed a statistically significant linear dependence between Chl_0 and IPP. The regression equation is

$$\log IPP = 1.62 + 0.40 \log Chl_0 \quad (R^2 = 0.12;\ N = 85;\ p < 0.01). \tag{9}$$

A weak correlation is explainable by the fact that IPP is limited by the incoming solar radiation and underwater PAR at the end of the growth season as well as low phytoplankton assimilation activity in the Kara Sea in the fall [27]. The leading role of the light factor in regulating the Kara Sea PP level is determined by the specific features of the optical properties of water, namely, high concentrations of dissolved (DOM) and particulate(POM) organic matter, low transparency, and a thin photosynthetic layer, as well as the season in which field studies are carried out. It is known that the role of the light factor in PP processes increases by the end of the growth season [21, 37, 59, 76]. Nonetheless, we believe it feasible to test the regression Chl_0–IPP model owing to the simplicity of this approach and to compare its precision assessment to the IPP prediction efficiency of the other two algorithms.

Depth-integrated Kara Sea PP model (Ψ-Mod). The works by Platt et al. [57, 60, 62], describing correlations between IPP, Chl_{ph}, and PAR, formed the theoretical basis for the Ψ-Mod. Initially, the Ψ-Mod was constructed using data for tropical, temperate, and polar regions of the World Ocean. The model was tested by PPARR1 [22]. The algorithm adapted for the Kara Sea includes the average values for the solar energy utilization efficiency in the water column ($\psi = P^b_{meas}/I_0$) [31] and the chl *a* vertical distribution index ($k = Chl_{ph}/Chl_0$) [22] as model coefficients. The input variables are Chl_0 and incident daily PAR. These characteristics may be rather easily recorded under field conditions. In this approach, IPP is calculable as

$$IPP_{mod} = k\psi\, Chl_0 I_0. \tag{10}$$

Since the distribution for the $k\psi$ product displays a pronounced lognormal pattern, it is purposeful to use a geometric mean [9], which amounts to 8.27 when averaged over the entire sea; correspondingly, Eq. (10) takes on the following form:

$$IPP_{mod} = 8.27 Chl_0 I_0. \tag{11}$$

Note that this computation algorithm was used earlier to study the IPP spatial variation in the Southern Ocean [5].

Empirical dependence between the chlorophyll concentration and Kara Sea PP (Chl_z_reg). The linear regression equation relating the logarithms of chl *a* concentration and PP at all depths is

$$\log PP_z = 0.43 + 1.13 \log Chl_z \quad (R^2 = 0.27;\ N = 355;\ p < 0.01). \tag{12}$$

This equation was used to compute PP_z according to the model curves of the vertical chl *a* distribution (see below). An analogous approach was applied by Hill et al. [39] for calculating PP in the Arctic. Note that the correlation between Chl_z and PP_z over the ARCSS-PP database was higher ($R^2 = 0.66$).

Approximation of vertical chlorophyll distribution curves and the Kara Sea PP depth-resolved model (KSDRM). The KSDRM utilizes the P^b_{opt} as well as underwater assimilation activity and chl *a* vertical curves. Daily IPP is calculated by integration over depth:

$$IPP_i = \int_z^0 P^b_z Chl_z DL(dz), \tag{13}$$

where P^b_z and Chl_z are the assimilation number and chl *a* concentration at depth *Z*, respectively, and *DL* is duration of the light day.

The P^b_z was calculated using its exponential dependence on PAR (I_z) expressed as the percentage of the maximum values:

$$P^b_{rel} = 11.65 I_z^{0.49}; \tag{14}$$

consequently,

$$P^b_z = P^b_{opt}\left((11.65 I_z^{0.49})/100\right). \tag{15}$$

The P^b_{opt} values were obtained from the empirical dependence of this characteristic on I_0 [27], where

$$P^b_{opt} = 10^{-0.71+0.901 \log I_0}. \tag{16}$$

By replacing P^b_{opt} from Eq. (16) with Eq. (15), we obtain

$$P^b_z = (10^{-0.71+0.901 \log I_0})\left((11.65 I_z^{0.49})/100\right). \tag{17}$$

The vertical chl *a* profiles were parameterized earlier [4]. Below we find the equations for the curves approximating the vertical chl *a* distribution for waters of different trophic levels.

Trophic gradation I ($Chl_0 = 0.1$–0.5 mg/m^3):

within the euphotic layer (1% PAR),

$$Chl_z = Chl_0((K_d z) + 68.96)/105.2, \tag{18}$$

and below the euphotic layer,

$$Chl_z = Chl_0((K_d z) - 17.47)/-19.95); \tag{19}$$

trophic gradation II ($Chl_0 = 0.5$–1.0 mg/m^3):

$$Chl_z = Chl_0 \exp(-(K_d z) + 0.08)/8.90), \tag{20}$$

trophic gradation III (Chl_0 = 1.0–2.0 mg/m^3):

$$Chl_z = Chl_0 \exp(-(K_d z) - 0.05)/6.52), \quad (21)$$

trophic gradation IV (Chl_0 > 2.0 mg/m^3):

$$Chl_z = Chl_0((K_d z) - 18.02)/-20.20). \quad (22)$$

Thus, it is possible to calculate the IPP within each trophic gradation of the water column using Eqs. (13), (17), and (18)–(22), respectively, instead of P_z^b and Chl_z. In this approach, Chl_0, I_0, and K_d are the model parameters.

Assessing model performance with regression analysis. Using the field data obtained in the Kara Sea as the input parameters, we assessed the precisions of regional Chl-based algorithms. The results of regression analysis are shown in Figs. 2 and 3 and Table 3. The model calculations fit the measured IPP values to an accuracy of 50–70%. The model relying exclusively on chl *a* distribution in the water column (Chl_z_reg) was the least predictive (R^2 = 0.50) (Table 3). The Chl_0_reg and Ψ-Mod algorithms performed better (R^2 = 0.65 and 0.69, respectively) as well as the depth-resolved (KSDRM) model (R^2 = 0.74).

An ideal algorithm, the precision assessment of which is described by the linear regression equation $y = b + ax$, displays a 1 : 1 ratio of the measured to calculated values (a = 1). The smallest a value (0.40) was obtained for the simplest IPP model based exclusively on the surface chl *a* concentration, Chl_0_reg (Fig. 2a). A better ratio of IPP_{mod} to IPP_{meas} (a = 0.98) was obtained by Ψ-Mod (Fig. 3a). Precision assessment of KSDRM gave a comparatively high coefficient a, 0.74 (Fig. 3b, Table 3). On average, Chl_0_reg and KSDRM overestimated IPP (B > 0), whereas Chl_z_reg and Ψ-Mod underestimated it (B = –0.03 and –0.25, respectively).

Regression error (RMSD) and model efficiency (ME). Table 3 lists the RMSD and ME values. The model performance data demonstrate that the algorithms that include photoadaptive parameters (Ψ-Mod) and taking into account the vertical chl *a* profiles (KSDRM) predict the in situ IPP values better (RMSD of 0.31 and 0.29, respectively) than models that take into account only the chl *a* concentration, Chl_0_reg and Chl_z_reg (RMSD of 0.32 and 0.42, respectively). This result is also confirmed by using ME as the indicator of model predictive capacity (Table 3).

DISCUSSION

In this paper, we described the results of developing regional models for the Kara Sea IPP and their skill assessment. Below we find the applicability potential and the degree of performance of the depth-integrated and depth-resolved models as well as the simplest and more complex models for assessing the Kara Sea IPP.

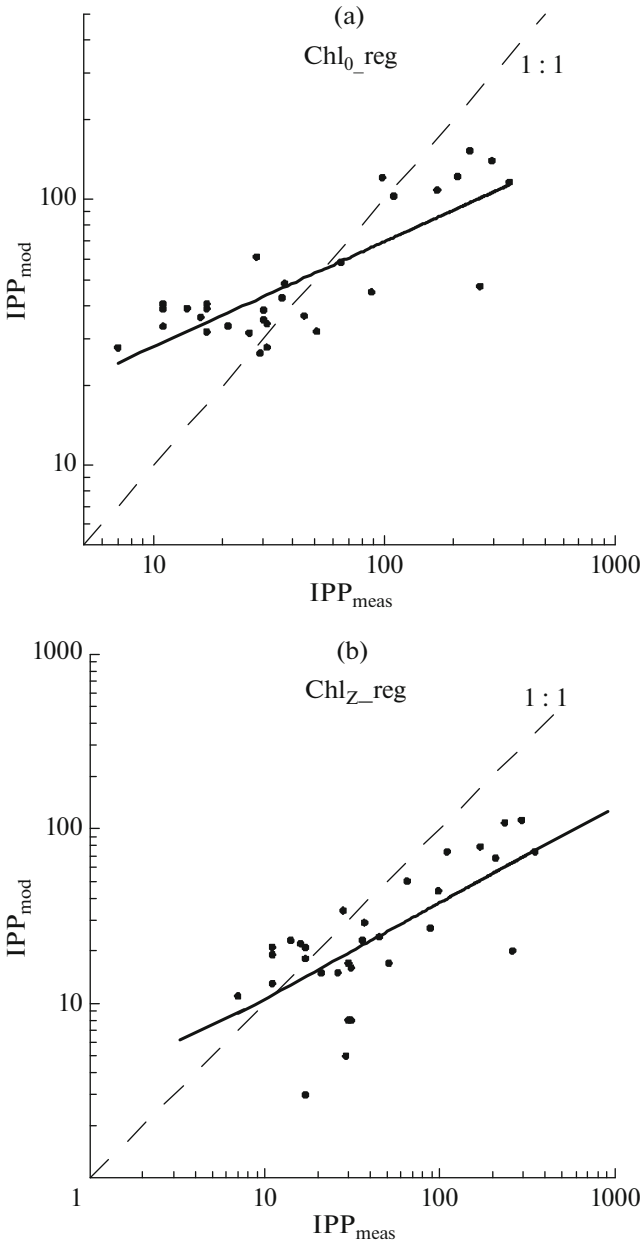

Fig. 2. Comparison of measured (IPP_{meas}, mg C/m^2/day) and calculated (IPP_{mod}, mg C/m^2/day) PP values in water column obtained using (a) Chl_0_reg and (b) Chl_z_reg models (see Table 2 for brief description of models).

Comparison of the depth-integrated and depth-resolved models. Our studies (Table 3) have not found any considerable differences in the IPP prediction accuracy between the WIDI and WIDR regional models (Ψ-Mod and KSDRM, respectively). Nonetheless, note that the depth-resolved model performed slightly better than the depth-integrated Ψ-Mod (RMSD = 0.29 and 0.31, respectively). On the other hand, the regional WIDI model, Ψ-Mod, gave the minimum bias (B = –0.03), while the WIDR algorithm (KSDRM) had a higher determination factor and effi-

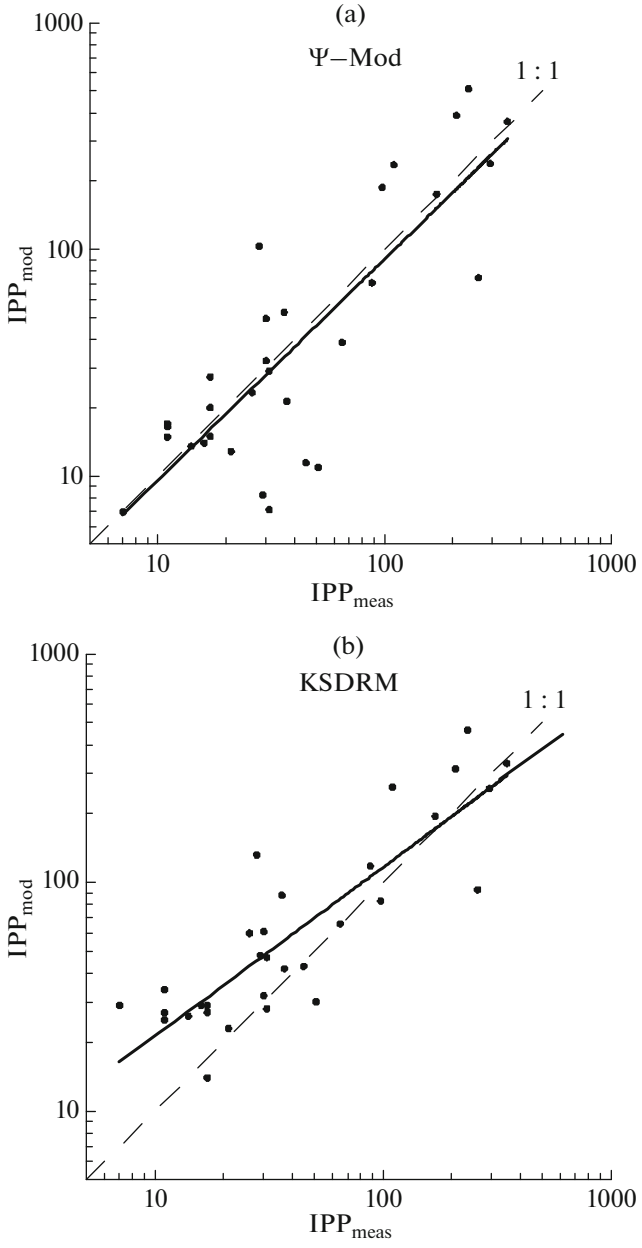

Fig. 3. Comparison of measured (IPP_{meas}, mg C/m^2/day) and calculated (IPP_{mod}, mg C/m^2/day) PP values in water column obtained using (a) Ψ-Mod and (b) KSDRM (see Table 2 for brief description of models).

ciency than Ψ-Mod (Table 3). The skill assessment of Chl_0_reg, Ψ-Mod, and KSDRM has shown that they either underestimated or overestimated the IPP by approximately twofold (RMSD varied from 0.29 to 0.32). The Chl_ζ_reg algorithm with its large regression error (RMSD = 0.42) was the exception (Table 3).

Saba et al. [65] have studied the correlation between model performance and station depth and demonstrated that the models usually underestimate the real IPP values for stations deeper than 4000 m and overestimate IPP at depths less than 750 m, while the calculation error increases with decreasing sampling depth. In general, our results agree with these data [65], since all the stations used in the Kara Sea for PP measurements were at depths <750 m.

As shown earlier, the vertical chl *a* profile taken into account in production models insignificantly improves the IPP computation results [17, 66]. The depth-integrated models explained ~85% of the IPP_{meas}, while the vertical variation in phytoplankton biomass and light intensity together accounted for only ~15% [17]. Development of regional models for the Kara Sea IPP has shown that the addition of data on chl *a* and P^b vertical distributions to the model equations improves the model performance (using RMSD and ME as accuracy index) by approximately 7% (Table 3). In addition, comparison of Ψ-Mod and KSDRM demonstrates that the former model insignificantly underestimates IPP_{meas} ($B = -0.03$), whereas the latter slightly overestimates in situ IPP values ($B = 0.17$).

Usually, the Arctic Ocean IPP models [63] assume that the vertical chl *a* distribution is homogeneous within the upper mixed layer (UML) and exponentially decreases below this layer [12]. A similar vertical pattern of chl *a* curves after "blooming" and its uniform distribution from the surface to the margin of photosynthetic layer before "blooming" were described by Hill and Zimmerman [40] in the Chukchi Sea. A uniform vertical chl *a* distribution in the photosynthetic layer was later used in the IPP estimates in the Arctic Ocean based on remotely sensed and field data [39]. Presumably, a more precise description of the chl *a* vertical profile is a necessary condition for increasing the efficiency of WIDR models.

The specific features in the chl *a* distribution in the Arctic Ocean may significantly influence the IPP value because of the deep chlorophyll maximum (DCM), which is frequently observed after "blooming" and either gives the secondary PP maximum or smoothes the vertical curve. The DCM and the resulting deep PP maximum influence the annual IPP values [10, 11, 48, 49]. As has been recently demonstrated, the DCM contribution to the Kara Sea IPP in the waters with different trophic status changes from 1 to 27% [27]. A poorly developed DCM and its small effect on the PP distribution in the water column are the specific features in the chl *a* vertical distribution in the Kara Sea. The averaged pattern has the chlorophyll maximum on the surface, while a decrease in the chl *a* concentration with depth is either linear or exponential depending on water productivity [4].

Comparison of simple chlorophyll-based models with models and algorithms utilizing incident PAR and photoadaptive parameters. Some empirical algorithms use chl *a* as the only parameter, allowing for estimation of the Arctic Ocean IPP because of the strong PP dependence on phytoplankton biomass [39, 40, 50]. These models regard the ratio of chl *a* concentration to

Table 3. Results of regression analysis of the correlation between IPP_{meas} and IPP_{mod} logarithms and efficiency characteristics of different models

Model	Regression statistics				Efficiency characteristics			
	a	*b*	R^2	*p*	*B*	σ	RMSD	ME
Chl_0_reg	0.40	1.05	0.65	<0.01	0.07	0.23	0.32	0.53
Ψ-Mod	0.98	0.01	0.69	<0.01	–0.03	0.56	0.31	0.58
Chl_z_reg	0.55	0.48	0.50	<0.01	–0.25	0.37	0.42	0.21
KSDRM	0.74	0.59	0.74	<0.01	0.17	0.41	0.29	0.62

a and *b*, coefficients in linear regression; R^2, determination coefficient; *p,* regression confidence interval; *B*, bias; σ, standard deviation; RMSD, root-mean-square-difference; and ME, model efficiency.

IPP as the simplest conversion factor without using any more complex parameterization involving the assimilation activity and efficiency of photosynthesis and PAR. Using the ARCSS-PP database, Hill et al. [39] discovered a close correlation between the logarithms of chl *a* concentration and PP for the entire depth range ($R^2 = 0.66$), which suggested that IPP could be predicted without involving photoadaptive parameters. This conclusion was confirmed by data obtained in the Beaufort Sea, showing the absence of any statistically significant correlation between PP and phytoplankton assimilation activity [38].

Our results demonstrate a less close correlation between Chl_z and PP_z ($R^2 = 0.27$). The use of surface chl *a* concentration as a direct characteristic for the Kara Sea PP also looks rather doubtful. The earlier regression analysis of the correlation between Chl_0 and IPP_{meas} suggests that only 12% of the IPP is explainable by variation in the surface chl *a* ($R^2 = 0.12$) [27]. Thus, the Chl_0 at the end of the growth season cannot be regarded as a characteristic of phytoplankton productivity in the water column. It has been also demonstrated that Chl_0 on the scale of the World Ocean accounts for <50% of the IPP [13, 14, 17]. On the other hand, the study of the IPP to P^b_{opt} ratio in the Kara Sea demonstrates that these parameters are closely correlated ($R^2 = 0.64$). In addition, IPP and P^b_{opt} mainly depend on the PAR level, which should be regarded as the main factor limiting the Kara Sea PP at the end of the growth season [27]. Thus, we expected that addition of P^b_{opt}, ψ, and I_0 to the algorithms for calculating IPP would improve their precision.

The model performance parameters shown in Table 3 demonstrate that Ψ-Mod and KSDRM, utilizing P^b_{opt}, and ψ as coefficients and I_0 as one of the input variables, provide better IPP prediction than algorithms utilizing only the chl *a* concentration. Note that of the models based on chl *a* alone, the predictive ability of the algorithm based on Chl_0 (Chl_0_reg) is higher than Chl_z_reg, which takes into account the vertical chl *a* distribution. On average, the predictive abilities of Ψ-Mod and KSDRM are 1.5 times better than that of Chl_z_reg (RMSD = 0.29, 0.31, and 0.42, respectively). The mean error of models (*B*) demonstrates that Ψ-Mod and Chl_z_reg underestimate whereas KSDRM and Chl_0_reg overestimate the observed IPP values. (Table 3). Hill and Zimmerman [40] inferred that the chl *a* models underestimate IPP in the Arctic Ocean, whereas Carr et al. [25] noted that the simplest Chl-based model [30] overestimates PP at high latitudes with low PAR and T_0 values.

CONCLUSIONS

Here we describe the developmentof region-specific models for the Kara Sea PP and the results of their efficiency. Our data demonstrate that the model predictive capacity can be improved by supplementing algorithms with photophysiological parameters, such as assimilation activity and photosynthetic efficiency, as model coefficients as well as PAR (and, to a lesser degree, vertical resolution) as an input variable. Thus, we regard the Ψ-Mod and KSDRM algorithms as optimal for predicting in situ IPP. In a future work, it will be necessary to compare the region-specific models and algorithms developed for other regions of the Arctic and World Oceans for their efficiency in predicting the Kara Sea IPP. The next stage in applying the developed algorithms to assess annual IPP values and long-term variation is the addition of remotely sensed data to the model equations. For depth-integrated region-specific algorithms, these parameters are Chl_0 and the daily PAR, and for the depth-resolved model, in addition, the diffusion attenuation coefficient (K_d) of the downwelling PAR.

Note that the region-specific algorithms developed for the Kara Sea display similar efficiencies to the earlier proposed models for other regions of the World Ocean [25, 32, 65, 66]. Predictive skill of these models has shown that they give either approximately twofold overestimated or twofold underestimated values as compared with the measured IPP. Comparison of the region-specific models with algorithms nonspecific to the Kara Sea in their efficiencies is a subject for future studies.

Lastly, it is necessary to mention the limitations of the above-described models. The analyzed algorithms are based exclusively on data for the fall season and should be used carefully to assess the IPP in other seasons. Thus, we propose to improve the production algorithms by expanding the experimental dataset on the phytoplankton production characteristics and developing models specific to different seasons.

ACKNOWLEDGMENTS

The work was supported by the Russian Foundation for Basic Research (project no. 13-05-00029); field studies were supported by the Russian Scientific Foundation (grant nos. 14-50-00095 under the problem "Ecosystems of Sea Regions Strategically Important for the Russian Federation" and 14-50-00095 under the problem "Interaction of Physical, Biological, and Geological Processes in the Coastal Zone, Coastal Water Areas, and Inland Seas"); and processing of the field material was supported by the Russian Scientific Foundation (grant no. 14-17-00681).

REFERENCES

1. V. I. Vedernikov, A. B. Demidov, and A. I. Sud'bin, "Primary production and chlorophyll in the Kara Sea in September 1993," Okeanologiya (Moscow) **34** (5), 693–703 (1994).
2. A. A. Vetrov and E. A. Romankevich, "Primary production and fluxes of organic carbon to the seabed in the Russian Arctic seas as a response to the recent warming," Oceanology (Engl. Transl.) **51** (2), 255–266 (2011).
3. M. E. Vinogradov, E. A. Shushkina, O. V. Kopelevich, and S. V. Shebestov, "Photosynthetic production of the World Ocean according to satellite and expedition data," Okeanologiya (Moscow) **36** (4), 566–575 (1996).
4. A. B. Demidov and S. A. Mosharov, "Vertical distribution of primary production and chlorophyll a in the Kara Sea," Oceanology (Engl. Transl.) **55** (4), 521–534 (2015).
5. A. B. Demidov, S. A. Mosharov, V. I. Gagarin, and N. D. Romanova, "Spatial variability of the primary production and chlorophyll a concentration in the drake passage in the austral spring," Oceanology (Engl. Transl.) **51** (2), 281–294 (2011).
6. S. A. Mosharov, "Distribution of the primary production and chlorophyll a in the Kara Sea in September of 2007," Oceanology (Engl. Transl.) **50** (6), 884–892 (2010).
7. I. N. Sukhanova, M. V. Flint, S. A. Mosharov, and V. M. Sergeeva, "Structure of the phytoplankton communities and primary production in the Ob River estuary and over the adjacent Kara Sea shelf," Oceanology (Engl. Transl.) **50** (5), 743–758 (2010).
8. M. V. Flint, T. N. Semenova, E. G. Arashkevich, I. N. Sukhanova, V. I. Gagarin, V. V. Kremenetskiy, M. A. Pivovarov, and K. A. Soloviev, "Structure of the zooplankton communities in the region of the Ob River's estuarine frontal zone," Oceanology (Engl. Transl.) **50** (5), 766–779 (2010).
9. J. Aitchison and J. A. C. Brown, "The lognormal distribution," Econ. J. **67**, 713–715 (1957).
10. M. Ardyna, M. Babin, M. Gosselin, et al., "Parameterization of vertical chlorophyll *a* in the Arctic Ocean: impact of the subsurface chlorophyll maximum on regional, seasonal and annual primary production estimates," Biogeosciences **10**, 1345–1399 (2013).
11. K. R. Arrigo, P. A. Matrai, and G. L. van Dijken, "Primary productivity in the Arctic Ocean: Impact of complex optical properties and subsurface chlorophyll maxima on large-scale estimates," J. Geophys. Res., C: Oceans Atmos. **116**, 11022 (2011). doi 10.1029/2011JC007273
12. K. R. Arrigo, G. L. van Dijken, and S. Bushinsky, "Primary production in the Southern Ocean, 1997–2006," J. Geophys. Res., C: Oceans Atmos. **113**, 08004 (2008). doi 10.1029/2007JC004551
13. W. Balch, R. Evans, J. Brown, et al., "The remote sensing of ocean primary productivity: use of a new data compilation to test satellite algorithms," J. Geophys. Res., C: Oceans Atmos. **97** (2), 2279–2293 (1992).
14. K. Banse and M. Yong, "Sources of variability in satellite-derived estimates of phytoplankton production in the Eastern Tropical Pacific," J. Geophys. Res. **95**, 7201–7215 (1990).
15. M. J. Behrenfeld, E. Boss, D. A. Siegel, and D. M. Shea, "Carbon-based ocean productivity and phytoplankton physiology from space," Global Biogeochem. Cycles **19**, GB1006 (2005). doi 10.1029/2004GB002299
16. M. J. Behrenfeld and P. G. Falkowski, "Photosynthetic rates derived from satellite-based chlorophyll concentrations," Limnol. Oceanogr. **42**, 1–20 (1997).
17. M. J. Behrenfeld and P. G. Falkowski, "A consumer's guide to phytoplankton primary productivity models," Limnol. Oceanogr. **42** (7), 1479–1491 (1997).
18. M. J. Behrenfeld, E. Marañon, D. A. Siegel, and S. B. Hooker, "A photoacclimation and nutrient based model of light-saturated photosynthesis for quantifying oceanic primary production," Mar. Ecol.: Progr. Ser. **228**, 103–117 (2002).
19. W. H. Berger, "Global maps of primary productivity," in *Productivity of the Ocean: Present and Past*, Ed. by W. H. Berger, (Wiley, Berlin, 1989), pp. 429–455.
20. R. R. Bidigare, B. B. Prezelin, and R. C. Smith, "Bio-optical models and the problems of scaling," in *Primary Productivity and Biogeochemical Cycles in the Sea*, Ed. by P. G. Falkowski and A. D. Woodhead (Plenum, New York, 1992), pp. 175–212.
21. S. Brugel, C. Nozais, M. Poulin, et al., "Phytoplankton biomass and production in the southeastern Beaufort Sea in autumn 2002 and 2003," Mar. Ecol.: Progr. Ser. **377**, 63–77 (2009).
22. J. Campbell, D. Antoine, R. Armstrong, et al., "Comparison of algorithms for estimating ocean primary production from surface chlorophyll, temperature, and irradiance," Global Biogeochem. Cycles **16**, (2002). doi 10.1029/2001GB001444
23. K. L. Carder, F. R. Chen, J. P. Cannizzaro, et al., "Performance of the MODIS semi-analytical ocean color

algorithm for chlorophyll *a*," Adv. Space Res. **33**, 1152–1159 (2004).

24. E. C. Carmack, D. Barber, J. Christensen, et al., "Climate variability and physical forcing of the food webs and the carbon budget on panarctic shelves," Progr. Oceanogr. **71**, 145–181 (2006).
25. M.-E. Carr, M. A. M. Friedrichs, M. Schmeltz, et al., "A comparison of global estimates of marine primary production from ocean color," Deep-Sea Res., Part II **53**, 741–770 (2006).
26. F. Colijn and L. Edler, *Working Manual and Supporting Papers on the Use of a Standardized Incubator-Technique in Primary Production Measurements* (HELCOM, Helsinki, 1999).
27. A. B. Demidov, S. A. Mosharov, and P. N. Makkaveev, "Patterns of the Kara Sea primary production in autumn: Biotic and abiotic forcing of subsurface layer," J. Mar. Sys. **132**, 130–149 (2014).
28. S. C. Doney, I. Lima, J. K. Moore, et al., "Skill metrics for confronting global upper ocean ecosystem-biogeochemistry models against field and remote sensing data," J. Mar. Sys. **76**, 95–112 (2009).
29. L. Edler, *Report of the ICES/HELCOM Workshop on Quality Assurance of Pelagic Biological Measurements in the Baltic Sea* (International Council for the Exploration of the Sea, Copenhagen, 1997).
30. R. Eppley, E. Steward, E. Abbott, and U. Heyman, "Estimating ocean primary production from satellite chlorophyll: introduction to regional differences and statistics for the Southern California Bight," J. Plankton Res. **7**, 57–70 (1985).
31. P. Falkowski, "Light-shade adaptation and assimilation numbers," J. Plankton Res. **3**, 203–216 (1981).
32. M. A. M. Friedrichs, M.-E. Carr, R. Barber, et al., "Assessing the uncertainties of model estimates of primary productivity in the tropical Pacific Ocean," J. Mar. Sys. **76**, 113–133 (2009).
33. V. V. Gordeev, "River input of water, sediment, major ions, nutrients and trace metals from Russian territory to the Arctic Ocean," in *The Freshwater Budget of the Arctic Ocean*, Ed. by L. L. Edward, (Kluwer, Amsterdam, 1998), pp. 297–322.
34. W. W. Gregg, P. Ginoux, P. Schopf, and N. Casey, "Phytoplankton and iron: validation of a global three-dimensional ocean biogeochemical model," Deep-Sea Res., Part II **50**, 3143–3169 (2003).
35. *Guidelines for the Measurement of Phytoplankton Primary Production. Baltic Marine Biologists Publication 1*, Ed. by G. Aertebjerg and A. M. Bresta (HELCOM, Helsinki, 1984).
36. D. Hanzlick and K. Aagaard, "Freshwater and Atlantic water in the Kara Sea," J. Geophys. Res. **85**, 4937–4942 (1980).
37. E. N. Hegseth, "Phytoplankton of the Barents Sea—the end of a growth season," Polar Biol. **17**, 235–241 (1997).
38. V. J. Hill and G. F. Cota, "Spatial patterns of primary production on the shelf, slope and basin of the Western Arctic in 2002," Deep-Sea Res., Part II **57**, 3344–3354 (2005).
39. V. J. Hill, P. A. Matrai, E. Olson, et al., "Synthesis of integrated primary production in the Arctic Ocean: II. In situ and remotely sensed estimates," Progr. Oceanogr. **110**, 107–125 (2013).
40. V. J. Hill and R. C. Zimmerman, "Estimates of primary production by remote sensing in the Arctic Ocean: assessment of accuracy with passive and active sensors," Deep-Sea Res., Part I **57**, 1243–1254 (2010).
41. H. J. Hirche, K. N. Kosobokova, B. Gaye-Haake, et al., "Structure and function of contemporary food webs on Arctic shelves: a panarctic comparison. The pelagic system of the Kara Sea—communities and components of carbon flow," Progr. Oceanogr. **71**, 288–313 (2006).
42. M. Jakobsson, A. Grantz, Y. Kristoffersen, and R. Macnab, "Bathymetry and physiography of the Arctic Ocean and its constituent seas," in *The Organic Carbon Cycle in the Arctic Ocean*, Ed. by R. Stein and R. W. Macdonald (Springer-Verlag, Berlin, 2004), pp. 1–6.
43. S. W. Jeffrey and G. F. Humphrey, "New spectrophotometric equations for determining chlorophylls *a, b, c1* and *c2* in higher plants, algae and natural phytoplankton," Biochem. Physiol. Pflanz. **167**, 191–194 (1975).
44. JGOFS, *Joint Global Ocean Flux Study Protocols (JGOFS), Core Measurement, Manual Guides* (UNESCO, Paris, 1994), pp. 119–122.
45. M. Jin, C. Deal, S. H. Lee, et al., "Investigation of Arctic sea and ocean primary production for the period 1992–2007 using a 3-D global ice-ocean ecosystem model," Deep-Sea Res., Part II **81–84**, 28–35 (2012).
46. O. I. Koblentz-Mishke, V. V. Volkovinsky, and Y. G. Kabanova, "Plankton primary production of the world ocean," in *Scientific Exploration of the South Pacific*, Ed. by W. S. Wooster (National Academy of Sciences, Washington, DC, 1970), pp. 183–193.
47. P. R. Makarevich, N. V. Druzhkov, V. V. Larionov, and E. I. Druzhkova, "The freshwater phytoplankton biomass and its role in the formation of a highly productive zone on the Ob-Yenisei shallows (southern Kara Sea)," in *Siberian River Run-Off in the Kara Sea*, Ed. by R. Stein, (Elsevier, Amsterdam, 2003), pp. 185–193.
48. J. Martin, J.-E.Tremblay, J. Gagnon, et al., "Prevalence, structure, and properties of subsurface chlorophyll maxima in Canadian Arctic waters," Mar. Ecol.: Progr. Ser. **412**, 69–84 (2010).
49. J. Martin, J.-E.Tremblay, and N. M. Price, "Nutritive and photosynthetic ecology of subsurface chlorophyll maxima in Canadian Arctic waters," Biogeosciences **9**, 5353–5371 (2012).
50. P. A. Matrai, E. Olson, S. Suttles, et al., "Synthesis of primary production in the Arctic Ocean: I. Surface waters, 1954–2007," Progr. Oceanogr. **110**, 93–106 (2013).
51. C. R. McClain, M. L. Cleave, G. Feldman, et al., "Science quality SeaWiFS data for global biosphere research," Sea Technol. **39**, 10–16 (1998).
52. C. R. McClain, G. Feldman, and S. B. Hooker, "An overview of the SeaWiFS project and strategies for producing a climate research quality global ocean bio-optical time series," Deep-Sea Res., Part II **51**, 5–42 (2004).
53. J. K. Moore, S. C. Doney, J. A. Kleypas, et al., "An intermediate complexity marine ecosystem model for

the global domain," Deep-Sea Res., Part II **49**, 403–462 (2002).

54. A. Morel and J.-F. Berthon, "Surface pigments, algal biomass profiles, and potential production of the euphotic layer: relationships reinvestigated in view of remote-sensing applications," Limnol. Oceanogr. **34**, 1545–1562 (1989).
55. E. M. Nöthig, Y. Okolodkov, V. V. Larionov, and P. R. Makarevich, "Phytoplankton distribution in the inner Kara Sea: a comparison of three summer investigations," in *Siberian River Run-Off in the Kara Sea*, Ed. by R. Stein, (Elsevier, Amsterdam, 2003), pp. 163–183.
56. J. E. O'Reilly, S. Maritorena, B. G. Mitchell, et al., "Ocean color chlorophyll algorithms for SeaWiFS," J. Geophys. Res. **103**, 24937–24953 (1998).
57. T. Platt, "Primary production of the ocean water columns as a function of surface light intensity: algorithms for remote sensing," Deep-Sea Res. **33**, 149–163 (1986).
58. T. Platt, C. L. Gallegos, and W. G. Harrison, "Photoinhibition of photosynthesis in natural assemblages of marine phytoplankton," J. Mar. Res. **38**, 687–701 (1980).
59. T. Platt, W. G. Harrison, E. P. W. Horne, and B. Irwin, "Carbon fixation and oxygen evolution by phytoplankton in the Canadian High Arctic," Polar Biol. **8**, 103–113 (1987).
60. T. Platt and S. Sathyendranath, "Oceanic primary production: estimation by remote sensing at local and regional scales," Science **241**, 1613–1620 (1988).
61. T. Platt and S. Sathyendranath, "Estimators of primary production for interpretation of remotely-sensed data on ocean color," J. Geophys. Res. **98**, 14561–14576 (1993).
62. T. Platt, S. Sathyendranath, C. M. Caverhill, and M. R. Lewis, "Ocean primary production and available light: further algorithms for remote sensing," Deep-Sea Res. **35**, 855–879 (1988).
63. S. Pabi, G. L. van Dijken, and K. R. Arrigo, "Primary production in the Arctic Ocean, 1998–2006," J. Geophys. Res., C: Oceans Atmos. **113**, 08005 (2008). doi 10.1029/2007/JC004578
64. J. E. G. Raymont, *Plankton and Productivity in the Oceans* (Pergamon, Oxford, 1967).
65. V. S. Saba, M. A. M. Friedrichs, D. Antoine, et al., "An evaluation of ocean color model estimates of marine primary productivity in coastal and pelagic regions across the globe," Biogeosciences **8**, 489–503 (2011).
66. V. Saba, S. Marjorie, M. A. M. Friedrichs, et al., "Challenges of modeling depth-integrated marine primary productivity over multiple decades: a case study at BATS and HOT," Global Biogeochem. Cycles **24**, GB3020 (2010). doi 10.1029/2009GB003655
67. SCOR–UNESCO, *Report of SCOR–UNESCO Working Group 17 on Determination of Photosynthetic Pigments in Sea Water: Monograph of Oceanography Methodology* (UNESCO, Paris, 1966), **Vol. 1**, pp. 9–18.
68. D. A. Siegel, T. K. Westberry, M. C. O'Brien, et al., "Bio-optical modeling of primary production on regional scales: The Bermuda Bio Optics project," Deep-Sea Res., Part II **48**, 1865–1896 (2001).
69. R. C. Smith and K. S. Baker, "The bio-optical state of ocean waters and remote sensing," Limnol. Oceanogr. **23**, 247–259 (1978).
70. E. Steemann-Nielsen, "The use of radioactive carbon (C^{14}) for measuring organic production in the sea," J. Cons. Perm. Inl Explor. Mer **18**, 117–140 (1952).
71. R. Stein, "Circum Arctic river discharge and its geological record," Int. J. Earth Sci. **89**, 447–449 (2000).
72. C. A. Stow, J. Jolliff, D. J. McGillicuddy, et al., "Skill assessment for coupled biological/physical models of marine systems," J. Mar. Sys. **76**, 4–15 (2009).
73. J. F. Tjiputra, M. Assmann, M. Bentsen, et al., "Bergen Earth system model (BCM-C): model description and regional climate-carbon cycle feedbacks assessment," Geosci. Model Dev. **3**, 123–141 (2010).
74. J. Uitz, H. Claustre, A. Morel, and S. B. Hooker, "Vertical distribution of phytoplankton communities in open ocean: an assessment on surface chlorophyll," J. Geophys. Res., C: Oceans Atmos. **111**, 08005 (2006). doi 10.1029/2005JC003207
75. T. Westberry, M. J. Behrenfeld, D. A. Siegel, and E. Boss, "Carbon-based primary productivity modeling with vertically resolved photoacclimation," Global Biogeochem. Cycles **22**, GB2024 (2008). doi 10.1029/2007GB003078
76. M. S. Yun, K. H. Chung, S. Zimmerman, et al., "Phytoplankton productivity and its response to higher light levels in the Canada basin," Polar Biol. **35**, 257–268 (2012).

Translated by G. Chirikova